FLAIR	**H2020**	
TE-KEVER	csem	DTU
Empa Materials Science and Technology		
NKT Photonics the power of light	NIT New Infrared Technologies	Radboud University Nijmegen
SenseAir Sensors for Life		

REPORT ON THE LIST OF RELEVANT INPUT PARAMETERS FOR WP4

FLAIR - FLying ultrA-broadband single-shot InfraRed Sensor
GA732968

Deliverable Information	
Deliverable Number: 3.1	**Work Package:** 3
Date of Issue: 16/04/2018	
Document Reference: 732968-FLAIR-D3.1-Report on the list of relevant input parameters for WP4	
Version Number: 1.0	
Nature of Deliverable: Report	**Dissemination Level of Deliverable:** PU
Author(s): Qing Pan, Frans J.M. Harren, et al	
Keywords: Parameters, IR sensor; air quality; greenhouse gases; airborne measurements;	

Abstract:
This document presents, qualitatively and quantitatively, a summary of relevant input parameters for WP4 identified by simulations and laboratory tests, covering various individual building blocks such as the supercontinuum laser source, the PbSe camera, the multipass cell, the gas handling system, the 2D spectrograph and imaging optics. A test instrument has been assembled at RU involving resources available within the WP3 framework. The performances of various commercially available sub-systems are compared, and emphasis has been put on parameters which are likely limiting the sensitivity and selectivity of the sensor to be assembled at CSEM within WP4.

Document History

Date	Version	Remarks
16/11/2017	0.1	First draft document
09/04/2018	0.2	Review from partners
16/04/2018	1.0	Final review and first issue

Document Authors

Entity	Contributors
RU	Frans J.M. Harren Qing Pan
CSEM	Gilles Buchs Tobias Herr
TEK	Afonso Mendes André Oliveira

Executive Summary

Task 3.1 of laboratory spectroscopy (WP3) involves spectroscopy data and preliminary gas analysis experiments of relevant species. The aim of this document is to summarize all the identified practical input parameters for WP4 through the knowledge obtained from a reference test setup assembled at RU. Various gas species of interest such as CO_2 and CH_4 have been measured, providing experimental feedback in comparison with simulations.

In order to support the sensor subsystem development and integration for WP4, the following aspects are focused in this document:

1) Absorption properties of various gases of interest;
2) Supercontinuum laser;
3) Multipass cell;
4) Gas handling system;
5) 2D spectrograph and imaging optics;
6) PbSe infrared camera;
7) Data processing algorithm.

In particular, parameters having high-risk impacts are highlighted. Fulfilling the requirements of these parameters will be essential to realize the goal of WP4 and eventually to validate the whole FLAIR concept.

The most important parameter directly influencing the minimum detectable gas concentration is the detectivity of the PbSe infrared camera, whose noise level is currently too high, limiting the **sensitivity** of the gas sensor. The overall instrumental spectral broadening is another important parameter affecting the resolvability of sharp absorption fingerprints. Detecting these fingerprint features is essential to the sensor's **selectivity** and reliability in presence of strong atmospheric interfering species such as water.

Note that parameters associated with UAV platform adaptation and sensor integration (WP5) are not subject to investigation within the framework of WP3.

Table of Contents

List of Tables

List of Figures

List of Acronyms

Acronym	Meaning
FPGA	Field-programmable Gate Array
FSR	Free Spectral Range
FWHM	Full Width at Half Maximum
TRL	Technology Readiness Level
UAV	Unmanned Aerial Vehicle
VIPA	Virtually Imaged Phase Array
WP	Work Package

Table 1 – List of acronyms.

1 Introduction

WP3 of the FLAIR project is dedicated to laboratory spectroscopy providing in-depth guidelines and feedbacks to other associated WPs. A synergetic involvement of all the consortium members through knowledge/experience exchange is essential to ensuring optimal performance of the FLAIR sensor. In particular, this document reports upon various important parameters identified in the laboratory environment. These parameters can have significant influence on the overall sensitivity, selectivity, reliability and detection speed of the sensor to be developed within WP4.

It should be noted that the experiments and simulations described herein leverage resources that are available at the laboratory level. Several commercially available products have been utilized in order to establish a reference for identification and for comparison purposes. The integration, adaptation and validation of the FLAIR sensor are subjects of subsequent WPs.

The structure of this document is organized in the following way. Firstly, the whole FLAIR sensor system is briefly reviewed, followed by an overview of the parameters associated with gas absorption properties. Parameters influencing the functionality of the spectrometer based on individual building blocks will also be discussed.

2 Procedure

This report was written by the participants listed in the table above under the lead of RU. More specifically, the following steps were taken:

- internal discussion meeting in Brussels (08.11.2017)
- establishment of the structure and first draft (16.11.2017)
- input from all participants received
- second report draft completed
- final feedback from all participants (09.04.2018)
- final report completed and submitted (16.04.2018)

3 Sensor overview

The overall sensor structure is schematically shown in Figure 1. Briefly, the supercontinuum laser (A) generates a broadband (2 – 5 µm or 8 – 12 µm) output beam propagating through a multipass cell (D) filled with air samples. The gas handling system (E) ensures proper control of the gas flow. The laser beam encoded with analyte absorption features is dispersed into a 2D pattern by a Virtually Imaged Phased Array (VIPA) and a conventional grating cross disperser. This pattern is imaged through the imaging optics (C) onto a photodetector array (B) and is further analysed by the data processing algorithm to reconstruct the absorption features of specific target gas species.

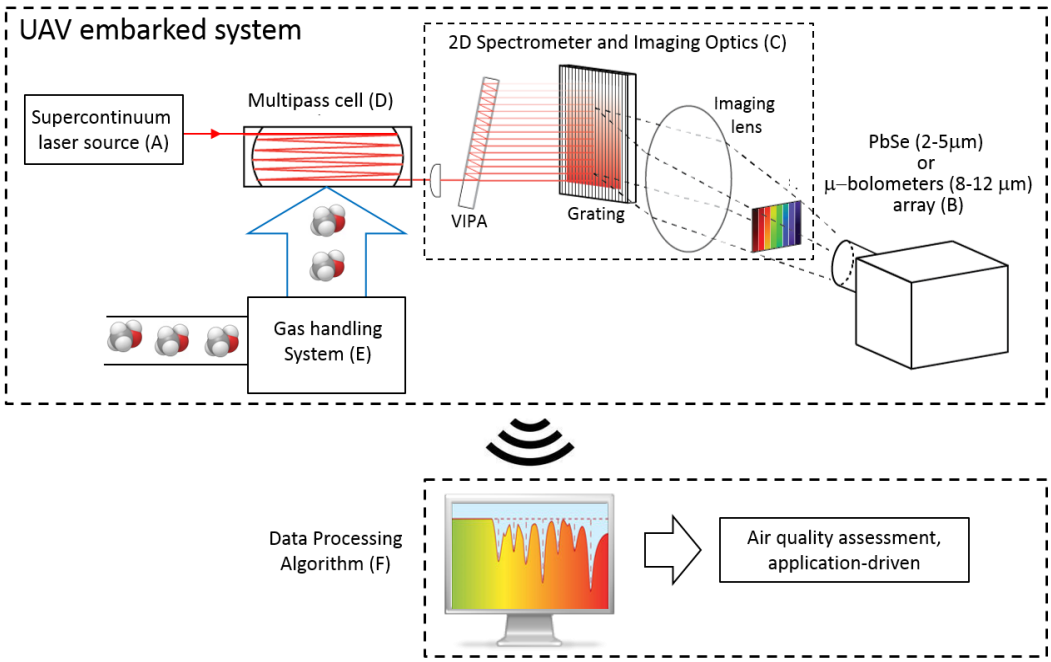

Figure 1. Simplified schematic diagram of the overall sensor system. Labels correspond to the subsystems descriptions in the text.

In practice, the sensor has to be assembled in a compact manner in order to match the interface with the UAV, as shown in the preliminary design from CSEM (Figure 2).

Figure 2. Preliminary design from CSEM showing the FLAIR sensor embedded in the payload of the UAV.

Remarkably, the FLAIR sensor is designed to resolve fingerprint absorption features with high resolution as supported by the high resolving power of the VIPA. Furthermore, broadband detection is also enabled through the utilization of the supercontinuum source in the 2 – 5 µm or 8 – 12 µm windows, allowing efficient detection of various gas species of interest.

4 Parameters associated with gas absorption

A reference database has been established for various target species for the test and validation phase (WP6). This database is presented in a separate deliverable, i.e. D3.2. At the present stage, several parameters have been identified from a pure spectroscopic point of view. For the following discussion, nitric oxide (NO) will be taken as an example to illustrate the importance of these parameters. The obtained conclusions can be applied to other gas species, while a complete determination of the optimal spectral working window for all these target species will be discussed in another separate deliverable D3.3.

4.1 The effect of spectral overlap

Even for the detection of a single target species (e.g. NO), the presence of atmospheric interference species (e.g. water) can significantly complicate the analysis as the absorption bands of these species can overlap. Figure 3A shows the absorbance spectra of NO and CO_2 at 1 ppm concentration (25 °C, 1 atmosphere, 1 meter path length). It is obvious that the strong CO_2 absorption in the >2660 nm region does not favour feasible detection of NO. Note that a typical CO_2 atmospheric concentration is at the level of 400 ppm.

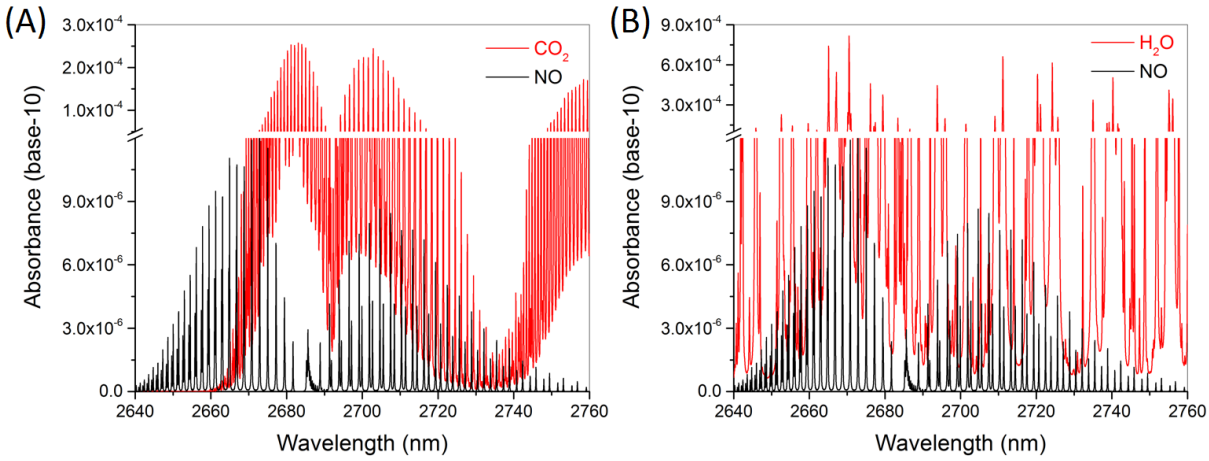

Figure 3. Absorbance spectra of NO with respect to CO_2 (A) and H_2O (B) at 1 ppm concentration.

The situation is even more complex when considering the inevitable water absorption as shown in Figure 3B. However, a closer examination of the absorption lines shows that it is still possible to distinguish NO from water, as illustrated in Figure 4.

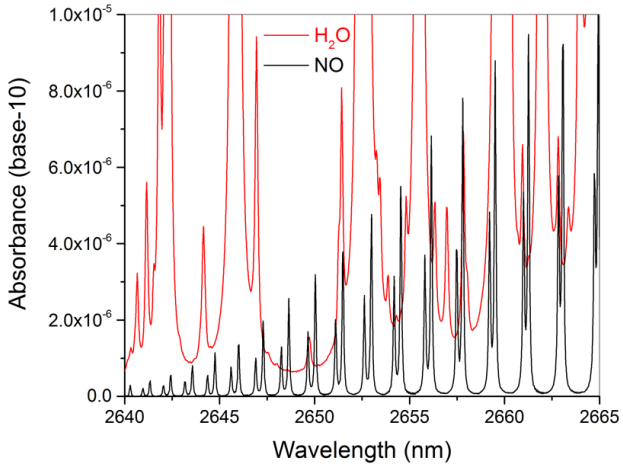

Figure 4. Zoomed-in absorbance spectra of NO with respect to H_2O at 1 ppm concentration.

Although heavily overlapping, the sharp absorption features at the vicinity of 2650 nm still allow exclusive detection of NO, provided that the relative concentration of water with respective to NO is low enough to avoid the overall water baseline overwrite. This constraint will therefore eventually set the detection limit of NO in the presence of interference species. Note that this constrain also defines the necessity to obtain high resolution of the spectrometer for reliable detection, as will be discussed in the next section.

4.2 The effect of instrumental broadening

As discussed in the previous section, the ability to resolve sharp absorption peaks is essential to reliable detection. Figure 5 quantitatively illustrates the influence of instrumental broadening on the absorbance line structure. Note that at high broadening level (i.e. 1 cm^{-1}), the overall intensity is low and the fine structure can no longer be resolved.

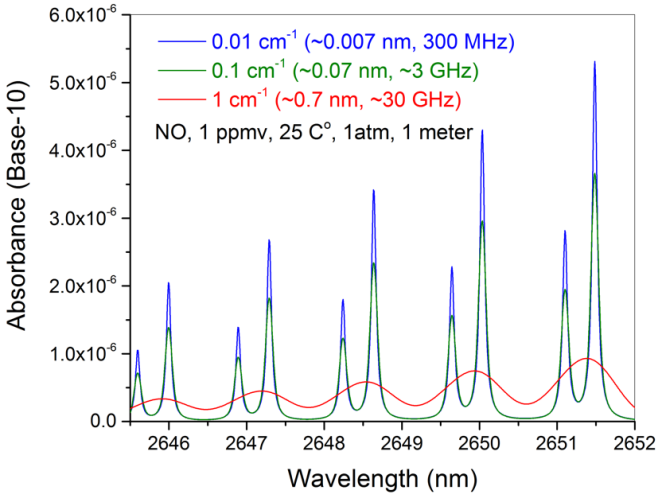

Figure 5. Absorbance spectra of NO at different instrumental broadening levels.

In principle, the FLAIR sensor resolution will be eventually limited by the VIPA bandwidth. Calculation has shown a Lorentzian lineshape. The VIPA at RU has an expected FWHM bandwidth of ~800 MHz, while the VIPA bandwidth at CSEM is ~350 MHz, which is sufficient to resolve the sharp absorption features of target species. In practice, however, it has to be noted that the final resolution is determined by all the broadening processes within the instrument. If the imaging optics are not limiting, the frequency interval corresponding to one pixel width at the detection plane should be convolved with the VIPA FWHM, yielding the final instrumental broadening.

4.3 The effect of pressure

Elevated pressure requiring a complex gas handling system can broaden or even distort the absorption lines. It is therefore not planned to operate the FLAIR sensor at pressures higher than one atmosphere. However, the pressure at operation will depend on the local atmospheric pressure influenced by the local altitude. This pressure has to be measured to correctly calculate the concentration with high precision. Furthermore, operating the detection cell at a fixed lower pressure (e.g. 100 mbar) would require a pump adding higher power consumption (and weight). At such a low pressure, high resolution is required as shown in Figure 6. It is therefore not recommended to measure the spectra at low pressures.

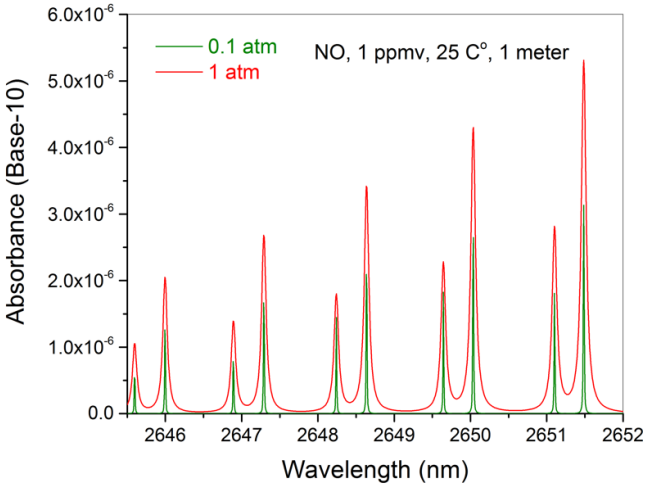

Figure 6. Absorbance spectra of NO at different pressures.

4.4 The effect of temperature

Generally speaking, temperature change can induce a change of the so called partition function and therefore influence the absorption line strength. In practice, however, this effect is not significant for a temperature fluctuation of ±10 °C as shown in Figure 7.

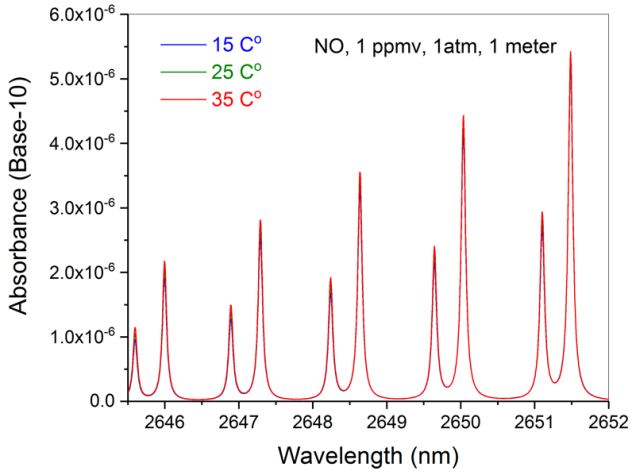

Figure 7. Absorbance spectra of NO at different temperatures.

Although the intrinsic absorption strength is weakly temperature dependent, it is however important to realize that temperature fluctuation can still deteriorate the performance of the FLAIR sensor by influencing the stability of the associated optical elements. This issue will be discussed in Section 5.2.

5 Parameters associated with individual subsystems

In this section, important parameters influencing the overall performance of the FLAIR sensor will be discussed at the individual subsystem level based on a test setup assembled at RU. In particular, the detectivity of the PbSe mid-infrared camera has been identified as the most important parameter for practical applications. More technical specifications can be found in deliverable document D2.3.

5.1 Supercontinuum sources

Two supercontinuum sources will be implemented into the FLAIR sensor for operations at two wavelength windows, i.e. 2 – 5 µm and 8 – 12 µm.

At the moment, only the 2 – 5 µm source has been delivered from NKT to RU and CSEM for test purposes, and NKT is targeting for a more compact system with less weight and power consumption. At the same time, the 8 – 12 µm source is also being developed at DTU with a finalization progress of ca. 35% (in October 2017). It is therefore not realistic to provide practical feedback regarding this source. However, experiences from the 2 – 5 µm source can still provide analogous insights to facilitate the development of the 8 – 12 µm source.

One of the most important parameters is the power density (mW/nm). This parameter is of particular importance for high resolution data acquisition as the supercontinuum beam is strongly dispersed by the 2D VIPA-grating disperser pair, resulting in less number of photons per detector pixel as compared to traditional 1D dispersion. This constraint is also closely related to the detectivity of the photodetector. In fact, the minimum detectable concentration C_{min} is influenced by the supercontinuum power I_0, the noise equivalent power (*NEP*) of the photodetector and the optical path length L via Equation (1).

$$C_{min} = \frac{NEP}{I_0 L \sigma} \tag{1}$$

where σ refers to the absorption cross-section and can be treated as an intrinsic property of a specific molecular species. From the above relationship, it is apparent that improving the I_o value by a factor of two can directly result in a two-fold improvement of the sensitivity.

Another important parameter is the spectral distribution of the power density. Figure 8 shows the two supercontinuum sources installed at RU and CSEM (in October 2017, official FLAIR source are expected for Spring 2018). For both of these two sources, high power densities are concentrated around 1.9 µm and 3.9 µm. It is therefore more favourable to detect gas species which have high absorption cross-section σ in these spectral regions. Analogously, species absorbing in the 2 – 3.5 µm region would be more difficult to detect. This issue will be discussed in more detail in document D3.2.

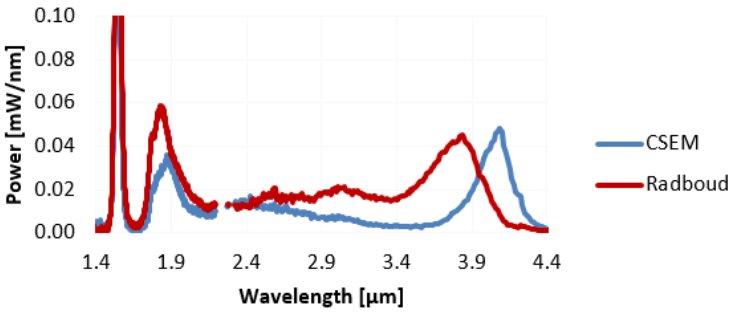

Figure 8. Power density spectra of the two supercontinuum sources installed at CSEM and RU.

In addition to the above issues, the repetition rate and stability are also important parameters influencing the detection speed and sensitivity. On the one hand, fast pulsing operation allows averaging over more pulses within a certain acquisition time (e.g. 1 s), effectively reducing the noise; on the other hand, slow drift of the laser system relaxes the necessity to frequently re-calibrate the reference spectrum. Furthermore, synchronizing the photodetector with the laser source can further reduce the noise.

5.2 Multipass cell

As shown in Equation (1), the optical path length L is an important parameter determining the minimum detectable concentration. In practice, high L value is achieved through multiple reflections between two mirrors of the sample cell. For instance, 30 reflections with a base distance of 33 cm would lead to an effective path length of ~10 m. At the moment SA is designing a compact multipass cell targeting 10 m path length, while at RU a commercial multipass cell AMAC-76 (shown in Figure 9) from Aerodyne Research Inc. has been aligned, achieving a ~10 m path length, allowing the detection of 5 ppm calibrated gas samples.

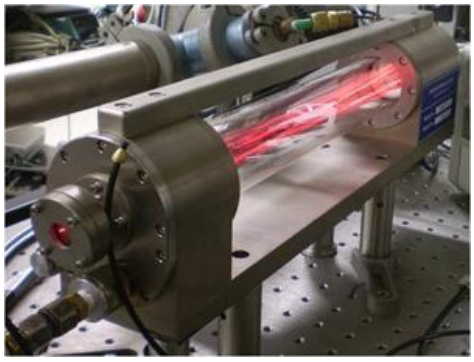

Figure 9. A test multipass cell aligned at RU for preliminary experiment purpose. The red beams are artificially inserted in order to highlight the multi-reflection property of this cell.

Due to weight and size constraints, the multipass cell shown in the above figure is not suitable for the FLAIR sensor (AR3 UAV). However, two important tradeoffs have been observed requiring careful engineering for the FLAIR multipass cell.

- Tradeoff between stability and size;
- Tradeoff between path length and power.

First of all, a more compact (i.e. small base length) design would naturally lead to more reflection passes inside the cell. Consequently, a small distortion of the mirrors due to thermal fluctuation and mechanical vibration would result in large misalignment of the pre-defined beam paths. In practice, the multipass cell can be stabilized in an oven to avoid the temperature influence. However, when the multipass cell is integrated into the UAV, unavoidable vibrations during flight may have significant impact of the beam path. It is therefore important to ensure that all the sensor components vibrate “in phase” in order to minimize the relative displacement.

Secondly, the non-unity reflectivity and high number of reflections would inevitably lead to power loss. As for the multipass cell tested at RU, ~20% laser power is lost because of 99.2% reflectivity and ~30 paths. Increasing the mirror reflectivity by sophisticated coating can reduce the power loss. However, it is very challenging to cover a broadband range (i.e. 2 – 5 or 8 – 12 μm). In addition, corrosive species such as SO_2 can also deteriorate the coating performance. It is therefore important to add protective coatings onto the mirror rather than only pursuing high reflectivity.

5.3 Gas handling system

The structure of the gas handling system strongly depends on the specific structure of the multipass cell, which is, in October 2017, still at the early stage of development. Therefore only general aspects will be discussed in this section.

As shown in Section 4.3, the absorption line bandwidth is pressure dependent, requiring performing the measurement at a constant pressure. From preliminary laboratory experiments, it is also observed that unstable gas flow can induce distortion to the baseline of the absorption spectra, possibly caused by flow-induced vibrations and change of the refractive index. It is therefore also important to keep steady state flow during measurement. In the laboratory environment this has been done by applying a commercial mass flow controller (Brooks, 5850E) and a gas flow controller (Bronkhorst, E7500-AAA) before and after the multipass cell, respectively. A pressure meter (Bronkhorst, P502C) and a dry scroll vacuum pump (Agilent Technologies IDP-2) are also connected to the cell outlet. For onboard application, however, this control system is not realistic concerning space and power constraints. Instead the flight-induced air flow could be used to also drive a continuous flow inside the multipass cell. This flow can monitored and controlled via a feedback valve system.

Limited by the design of the multipass cell, the flow direction is along the base length of the cell in the laboratory environment, causing instability when switching gas samples. This effect can be minimized by directing the gas perpendicular to the mirror axis of the multipass cell. In practice, Teflon tubing is recommended for the multipass cell inlet in order to prevent molecules from sticking on the inner surface of the tube. A filter to remove strong interfering species such as water vapour may be also applied.

Depending on the stability of the multipass cell, the reference baseline spectra may be regularly re-measured. More specifically, the absorbance A (i.e. optical density) of a certain molecular species at wavelength λ, by definition, is determined by laser power before (I_0) and after (I_T) passing through the gas species of interest, as shown in Equation (2).

$$A(\lambda) = log_{10}(\frac{I_0}{I_T}) \quad (2)$$

If the drift of the multipass cell causes significant changes to the reference I_0, it is necessary to measure I_0 in time before this drift jeopardizes $A(\lambda)$. This recalibration can be done by pumping the gas cell and refilling it with non-interfering gases, such as dry N_2. However, this procedure will increase the complexity of the gas handling system and should be avoided.

If the drift of the multipass cell is negligible, the supercontinuum and spectrometer drifts can be corrected by applying a reference beam path bypassing the multipass cell. This issue will be discussed in the next section.

5.4 2D spectrograph and imaging optics

As pointed out in Section 4.2, the resolution is an important parameter directly influencing the sensitivity of the FLAIR sensor. High resolution is obtained by leveraging the high angular dispersion property of the VIPA. Generally speaking, a thicker VIPA grants a better resolution, but at the same time results in a lower free spectral range (FSR), demanding better grating optics in order to efficiently separate the overlapping patterns. In other words, the VIPA resolution sets the upper limit for the 2D spectrograph, provided that the grating resolution is sufficient to resolve one VIPA FSR. At CSEM, a preliminary CAD design has been performed as shown in Figure 10. A 20 cm focal lens has been found necessary to

efficiently distinguish the overlapping stripes. In practice, this sensor system should also be purged with dry N_2 in order to avoid interfering absorption (such as water vapour and CO_2) in the beam path (rather than in the multipass cell).

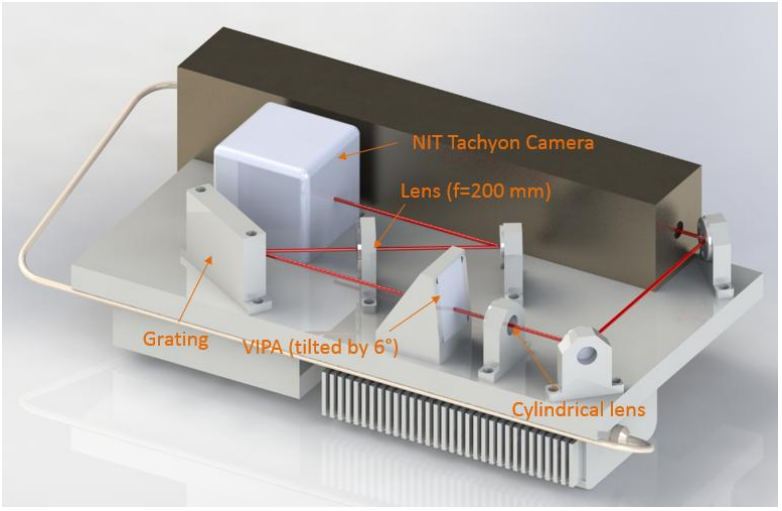

Figure 10. Preliminary design of the whole FLAIR sensor system from CSEM.

It requires attention that in order to capture the full spectral band (i.e. 2 – 5 µm and 8 – 12 µm), large-size camera and optics are required. Alternatively, the grating should be rotated. Furthermore, large chromatic aberration should be avoided considering the broadband nature of the supercontinuum source. Due to these limitations (as well as due to limited the spectral content of the super-continuum), the above CAD design only covers a spectral bandwidth of ca. 300 nm. Considering the fact that different gas species absorb in different spectral windows, it is more realistic to target only one or two species of interest at the first stage for test and validation purposes. Also note that the applicability of the VIPA strongly depends on the high reflectivity of the front coating. At the moment two different VIPAs with different spectral coverage are tested at CSEM (4 µm – 5 µm) and RU (2.4 µm – 4.5 µm). As the supercontinuum output power density is inhomogeneous and shows more power around 4 µm, it is more practical as a starting step to test CO_2 which absorbs strongly around 4.3 µm.

As also mentioned in Section 5.3, reference recalibration may be also required depending on the stability of the spectrometer. If the multipass cell drift is negligible, a reference beam path can be achieved by utilizing a beam splitter pair and shutter. This concept is schematically shown in Figure 11.

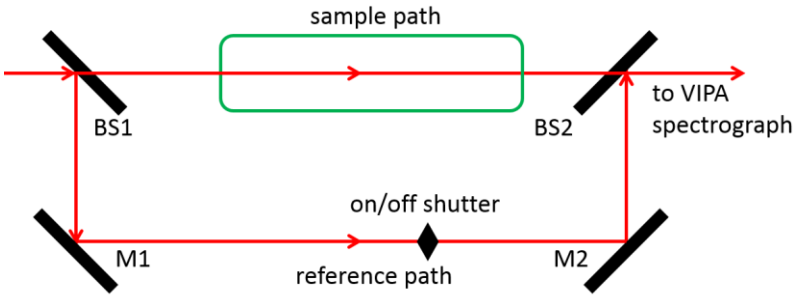

Figure 11. Possible alignment concept showing a parallel reference beam path allowing drift correction of the supercontinuum and the VIPA spectrometer (BS: beam splitter; M: mirror).

A drawback of the above design is that a significant portion of the supercontinuum power would be lost by splitting the beam. Flip mirrors can be also used to replace the beam splitters, but mechanical stability may be problematic. In case the VIPA spectrograph is both thermally and vibrationally stabilized and there is negligible crosstalk between different wavelength components of the supercontinuum, then the above alignment can be simplified by replacing M1 by a single point detector monitoring only the power. Alternatively, a number of specific pixels of the camera can be utilized as reference pixels to correct possible drift of the recorded power. Note that, in this case, these pixels must remain unaffected by gas absorption. In other words, these pixels must be selected in such a way that their corresponding wavelength components reside outside of the gas absorption windows.

At RU, the VIPA has been tested in combination with a diffraction grating (Thorlabs, GR2550-45031). A 3-inch gold parabolic mirror (Thorlabs, MPD399-M03), instead of a spherical lens, has been placed after the grating in order to avoid chromatic aberration and to capture as much light as possible. The results are shown in Figure 12. A single vertical stripe is observed due to the overlap of different wavelength components. This quasi-1D feature is expended into a 2D pattern by a grating cross disperser. A commercial thermopile array (HTPA 80x64d, Heimann Sensor) has been used for image acquisition.

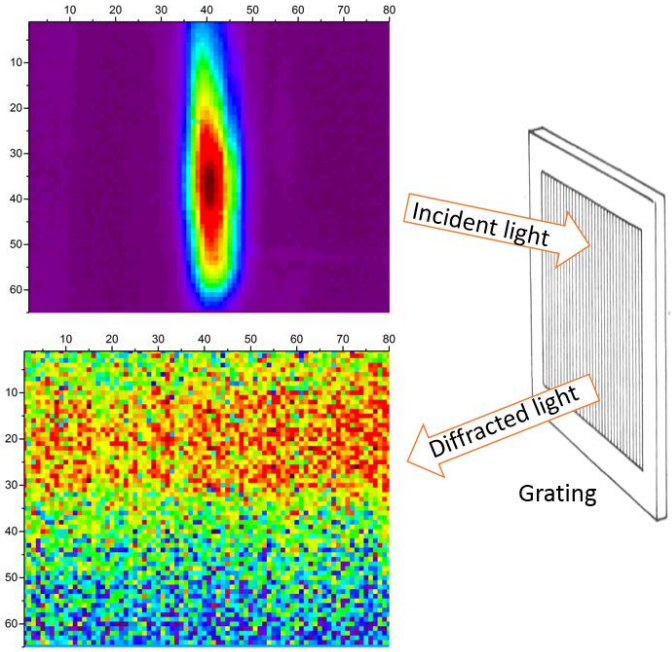

Figure 12. Recorded VIPA output pattern before (top image) and after (bottom image) the grating cross disperser. For simplicity, the off-axis parabolic mirror (acting as a focusing lens after the grating) is not shown.

The most important observation is that the signal-to-noise (S/N) ratio after grating cross dispersion is only ~3 even at full power operation of the supercontinuum. This problem is caused by the following three main factors:

1) Low detectivity of the uncooled infrared camera.
2) Power loss from the VIPA.
3) Power loss from the grating.

The first limitation will be discussed in more detail in Section 5.5, whereas the VIPA-induced power loss was identified as high as 50%. Furthermore, a significant fraction of the remaining

power (~40%) was also consumed by the 0th diffraction order of the grating. Consequently, the obtained 2D spectral pattern is far from any practical applications.

The above problem can be solved by utilizing a cooled (77 K) InSb camera, but the complexity and cost will be significantly increased. Alternatively, at RU, the detectivity bottleneck has been circumvented by up-converting the mid-infrared spectra into the near-infrared, allowing leveraging an efficient CCD camera (80% quantum efficiency). Details about this technique are beyond the scope of this document. More technical information can found from references 1 and 2. Unfortunately, this up-converting method is not suitable for the FLAIR application due to various constraints such as space, weight and power budget. Nonetheless, it has been identified in the laboratory environment that the drift of the supercontinuum (on a time scale of seconds) is likely the next limiting factor for the sensitivity. More specifically, a noise equivalent absorbance of the order of 10^{-4} has been achieved, limited mainly by the laser drift. This noise level corresponds to the absorption of 5 ppm ethanol close to the detection limit, as shown in Figure 13.

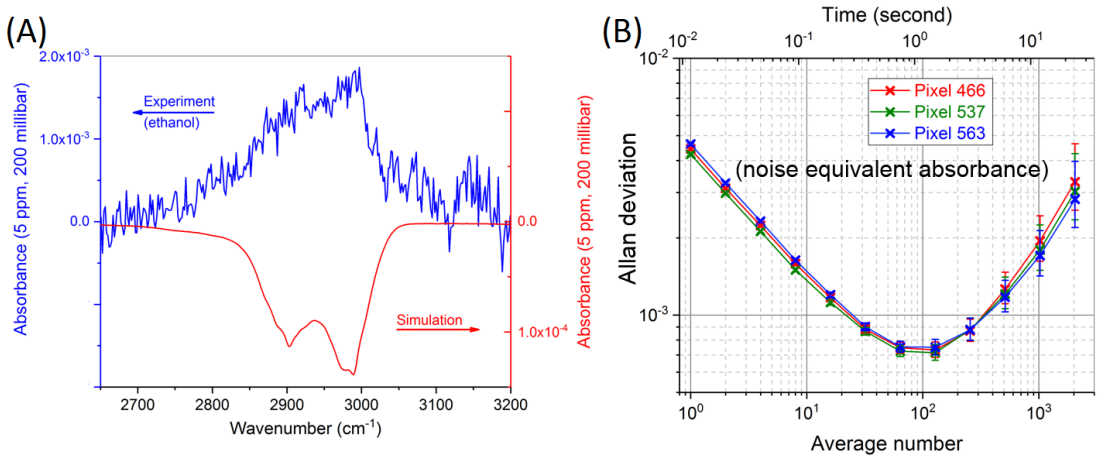

Figure 13. (A) Experimental and simulated absorbance spectra of 5 ppm ethanol, agreeing with the associated Allan deviation (B) showing a noise equivalent absorbance on the order of 10^{-4} at 100 averages. Note that the Allan deviation increases after this averaging number due to drift of the supercontinuum laser.

5.5 PbSe infrared camera

As shown in the previous section, the detectivity of the infrared camera is the most important factor currently limiting the VIPA spectrometer from practical applications. In principle, an uncooled PbSe detector should achieve a detectivity on the order of 10^8 cm·Hz$^{1/2}$/W in the 2 µm – 5 µm window; in practice, however, the detectivity of the current NIT camera is likely one order of magnitude lower than the expected value. NIT is at the moment developing a new camera version with an expected one order of magnitude improvement of the detectivity. As for the 8 µm – 12 µm region, PbSe camera would not be applicable. A thermopile or bolometer array can be instead used. Note that these detectors should ideally also have a 10^8 cm·Hz$^{1/2}$/W detectivity.

In addition to the detectivity, camera readout drift should also be minimized. Figure 14 shows a typical PbSe camera output of a single pixel with and without illumination at 3041.7 nm recorded at RU. Note that the dark baseline drifts up whereas the photo-signal drifts down. This systematic drift must be avoided or corrected in order to allow useful averaging of the raw data. When pulsed light is applied, more sophisticated output has been observed, which is beyond the scope of this document and is still under investigation.

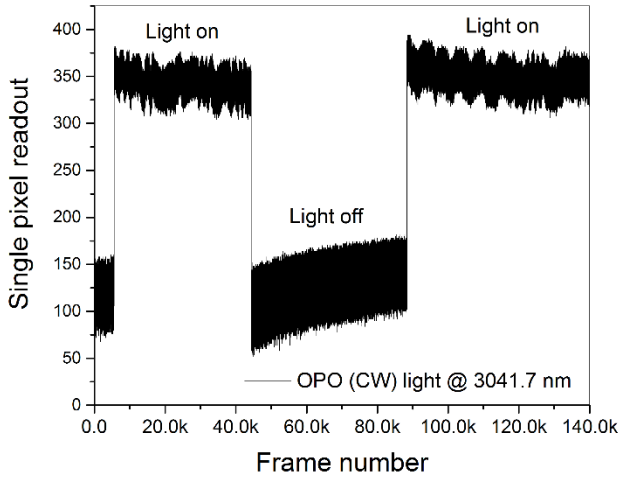

Figure 14. Readout of a single pixel at 500 Hz frame rate.

The above figure also shows that the dark noise is as high as ~50 counts. Since the maximum readout count is 1024, the low dynamic range would also likely limit the sensitivity accuracy and detection range of the FLAIR sensor.

One advantage of PbSe cameras over thermopiles is the detection speed. NIT is currently developing a new version with a possible frame rate of 2 kHz. For comparison, the thermopile sensors are much slower with a typical frame rate of ~10 Hz. The fast detection speed of PbSe camera allows versatile signal processing methods to reduce noise, as will be discussed in the next section.

5.6 Data processing algorithm

The test camera at RU has a maximum frame rate of 500 Hz. Note that this frame rate is not sufficient to capture individual pulses of the supercontinuum, which is at 40 kHz. It has been found that real-time signal processing with LabVIEW can reduce the noise. Two methods have been tested so far at RU:

1) Raw data averaging
2) Cross correlation

As the first method is rather straightforward, the second method is based on the assumption that the noise is completely random and therefore its cross correlation with a known reference waveform tends to vanish. In practice, unfortunately, both of these two methods lead to insufficient correction due to systematic drift of the camera. Note that this drift is different for different pixels. This phenomenon is also known as non-uniformity.

Although complete correction of this drift is not realistic, it is still of high importance to ensure that the camera (and ideally other sensor components) is drift free within a certain time interval. Then a fast data processing algorithm can be developed to finalize the measurement within this short period of time, followed by a re-calibration of the reference spectrum.

Chip-level signal processing by using a field-programmable gate array (FPGA) may be considered for fast calculation. Pattern recognition leveraging powerful artificial intelligence (machine learning) technology may also offer new possibilities for efficient and reliable sensing targets. Depending on the specific design and operation of the sensor hardware, at this stage of research these issues remain open to discussion.

6 Summary

The following list summarizes the identified input parameters for WP4 according to the above discussion. These parameters are obtained based on a test setup assembled at RU. It should be noted that the final FLAIR sensor structure can still deviate from its initial design, and a successful measurement relies on a synergetic operation of all the individual building blocks of the FLAIR sensor. New factors such as vibration are also expected to influence the sensor performance and will be investigated in future research.

- **Gas absorption properties**

  Spectral overlap, absorption line shape (resolution dependent), pressure, temperature.

- **Supercontinuum laser**

  Power density, spectral distribution, stability.

- **Multipass cell**

  Effective path length, stability, power loss.

- **Gas handling system**

  Pressure, flow stability, flow direction.

- **2D spectrograph and imaging optics**

  Power loss, resolution, detection range, reference beam path (possible), N_2 purge.

- **PbSe infrared camera**

  Detectivity/noise (most important), dynamic range, drift, non-uniformity, interaction with pulsed light (open question), speed.

- **Data processing algorithm**

  Noise reduction, pattern recognition (remains open at this stage).

7 References

[1] J. S. Dam, P. Tidemand-Lichtenberg, C. Pedersen, *Nature Photonics* 6, 788–793 (2012).

[2] A. Barh, C. Pedersen, P. Tidemand-Lichtenberg, *Optics Letters* 8, 1504–1507 (2017).